Capttery: Scalable Battery-like Room-level Wireless Power

Chi Zhang*
c4zhang@ucsd.edu
UC San Diego

Sidharth Kumar*
sidharthpunia10500@gmail.com
IIT Delhi

Dinesh Bharadia
dineshb@ucsd.edu
UC San Diego

ABSTRACT

Internet-of-things (IoT) devices are becoming widely adopted, but they increasingly suffer from limited power, as power cords cannot reach the billions and batteries do not last forever. Existing systems address the issue with ultra-low-power designs and energy scavenging, which inevitably limit functionality. To unlock the full potential of ubiquitous computing and connectivity, our solution uses **cap**acitive power transfer (CPT) to provide ba**ttery**-like wireless power delivery, henceforth referred to as "Capttery". Capttery presents the first room-level (~5 m) CPT system, which delivers continuous milliwatt-level wireless power to multiple IoT devices concurrently. Unlike conventional one-to-one CPT systems that target kilowatt power in a controlled and potentially hazardous setup, Capttery is designed to be human-safe and invariant in a practical and dynamic environment. Our evaluation shows that Capttery can power end-to-end IoT applications across a typical room, where new receivers can be easily added in a plug-and-play manner.

KEYWORDS

wireless power transfer (WPT), capacitive power transfer (CPT), Internet-of-Things, energy harvesting

ACM Reference Format:
Chi Zhang, Sidharth Kumar, and Dinesh Bharadia. 2019. Capttery: Scalable Battery-like Room-level Wireless Power. In *The 17th Annual International Conference on Mobile Systems, Applications, and Services (MobiSys '19), June 17–21, 2019, Seoul, Republic of Korea.* ACM, New York, NY, USA, 13 pages. https://doi.org/10.1145/3307334.3326077

1 INTRODUCTION

The vision for IoT is to enable us to *measure* and *control* our surroundings, in a *ubiquitous*, *reliable*, *coordinated*, and *intelligent* manner. To achieve such a vision, these devices require processing power backed by uninterrupted wireless connectivity and untethered energy sources. The limited growth of battery capacity [56] has thus fueled long and ongoing quests for ultra-low-power processing and connectivity.

The improvement in energy efficiency eventually diminishes, and the stringent energy budget inevitably limits *functionality*, *reliability*, and *interoperability*. For example, to achieve μW-level connectivity, one has to use modified backscatter MAC/PHY protocol [15, 29, 53], must stay within meters of a feeding access point (AP) [15, 29, 53], and cannot process the data with sophisticated algorithms. In contrast, standard Wi-Fi and Bluetooth devices do not have such limitations, but they require mW-level power[1]. If we can achieve *milliwatt-level continuous* wireless power transfer (WPT) in *dynamic and human-safe* environments, with *room-level* coverage, and allow the *addition of multiple devices seamlessly* with no reduction in power transfer per device, then the usability of IoT devices would be significantly improved.

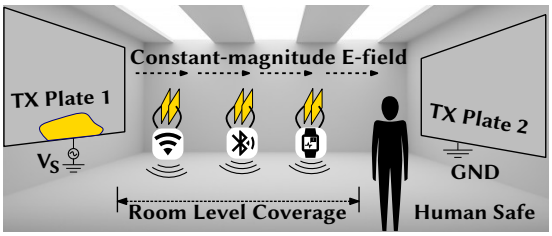

Figure 1: Overview of Capttery. Capttery uses insulated metal plates to create a constant-magnitude electric field, and couples capacitively to deliver milliwatts of power across the room. The E-field can power communication and computation for tens of IoT devices concurrently.

Unfortunately, current WPT systems fail to satisfy these requirements. Inductive power transfer (IPT) uses magnetic fields to convey watts of power. But due to the closed nature of the field, the distance is limited to below one meter even for the cutting-edge [48]. It also struggles to support multiple devices in a scalable manner [30]. A recent advance over IPT, the quasi-static cavity resonance (QSCR) [16–18, 47], extends the range to a few meters, but requires the whole space to be enclosed by metal. RF-based power transfer achieves longer range, at a few meters [4], but with an omnidirectional antenna power quickly diminishes with distance, to less than a μW at a meter. A natural question arises: can we provide milliwatts of continuous wireless power, for room-level coverage, to 10s of centimeter-sized IoT devices in a simple and scalable manner?

In this paper, we show that capacitive power transfer (CPT) can meet the above requirements. The key insight is that CPT uses electric fields to deliver power wirelessly, which, unlike closed magnetic fields, are open by nature. This allows the field to be stretched across the room for an extended range of power transfer, while maintaining constant magnitude without extensive infrastructure. However, previous CPT systems did not leverage the open nature, and only work at very short distances (< 10 cm) for applications such as electric vehicle (EV) [21] charging. Our work, Capttery (Fig. 1), presents a new architecture and design to make CPT work at *distances of multiple meters* and ensure *continuous mW-level power*

*Co-primary authors.

[1]Peak power consumption can be high, but a duty-cycled Wi-Fi radio can operate within milliwatt average power at low data rates.

MobiSys '19, June 17–21, 2019, Seoul, Republic of Korea

ACM ISBN 978-1-4503-6661-8/19/06…$15.00
https://doi.org/10.1145/3307334.3326077

to multiple devices. Furthermore, Capttery is the first *human-safe* CPT system that *works in uncontrolled environments*.

To maintain a human-safe constant-magnitude electric field over long distances and deliver power to centimeter-sized IoT devices, Capttery needs to overcome multiple challenges: *(i.)* The long distance and small receiver size make the coupling between the transmitter and the receiver extremely weak, making it challenging to deliver continuous milliwatt-level power. *(ii.)* Previous CPT systems produce unsafe levels of electric fields, and the operation stops when foreign objects are detected [58]. However, this mode of operation does not work for IoT devices, as humans need to live within the room coverage. Therefore, Capttery needs to ensure the electric field is controlled and human-safe. *(iii.)* In conventional CPT systems, change in the receiver would disturb the operation of the transmitter, which precludes adding new and mobile receivers in a plug-and-play way.

To overcome these challenges, Capttery presents design and optimization of the matching networks on both the transmitter and receivers, while being the first to consider the safety limit on electric fields. Furthermore, we design the transmitter such that it is insensitive to receiver characteristics and environmental dynamics. Together, this allows our system to deliver over 20 mW at more than 1 m distance, and provide mW-level power to 10s of receivers simultaneously, while increasing the number of receivers does not significantly decrease power transfer or require any adjustment. Furthermore, with only two plates of size 60 cm × 90 cm it can deliver at least 1 mW of power with 4.4 m range and at least 1.2 m lateral coverage. Our contribution is summarized as follows:

- Capttery is the first long-range and safe CPT system for IoT devices. Also, we give closed-form formulas and clear guidelines for designing and implementing such systems.
- Capttery explores CPT for multiple receivers by designing an invariant transmitter and modeling/simulating its performance through controlled experiments.
- We design measurement methods and equipment specifically for long-range CPT to avoid falsely high power readings.
- We design, implement, and evaluate Capttery extensively in realistic settings, including two showcase applications.

We deploy Capttery in realistic environments, with panels of size 60 cm × 90 cm covered by kitchen foil as TX plates and 10 receivers. Our evaluation shows:

- Capttery can deliver continuous power of 20 mW at 1 m and 1 mW at 4.4 m in a human-safe environment, which is a first for CPT systems and 3 orders of magnitude greater than RF-based systems, while the RX plates can be as small as 5 cm × 6 cm.
- Presence of large metal objects does not hinder Capttery's operation, and the coverage extends beyond the physical size of the TX plates.
- We deploy 10 receivers in centimeter/decimeter scale and observe that each of them receives continuous power transfer of at least 1 mW at 1.9 m, which totals to 26.5 mW of continuous power.
- Finally, we bundle the CPT receiver with showcase applications that harvest power continuously at 1.9 m distance and store it in a capacitor. This allows us to power a UWB localization tag, which performs both wireless transmission and computations to achieve decimeter-level localization at a 10 Hz rate, and a low-power BLE sensing tag that requires continuous 2 mW power to operate.

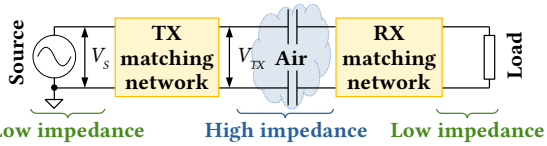

Figure 2: General structure of CPT systems.

Finally, we note the major limitation of Capttery: its end-to-end efficiency is 0.74% at 1.9 m. This efficiency, however, is over 1000× better than RF power transfer, but nearly 100× worse than IPT/QSCR (Sec. 9). Infrastructure required for RF power transfer is typically readily available, while QCSR requires a metal cage. In contrast, Capttery forms a middle ground, requiring just a set of metal plates while providing sufficient power for IoT devices. We believe future optimizations in circuits and architecture will significantly improve the efficiency figure. Capttery opens up a new avenue for future research where a simple deployment of metal plates in the walls could enable the vision of wirelessly-powered IoT devices.

2 BACKGROUND: CONVENTIONAL CPT

The traditional design of capacitive power transfer (CPT) system was for applications such as electric vehicle charging [21, 37], where no object is allowed in the narrow gap between the TX and the RX. The overall concept of capacitive power transfer (CPT) systems is shown in Fig. 2, where 2 TX plates deliver AC power to 2 receiver plates, through the loop formed by capacitances between the plates. Since the coupling capacitances are usually in the pF or sub-pF range, a large voltage V_{TX} across the TX plates can only deliver a small current, and thus small power to the RX. To effectively push power through such a high impedance, CPT systems employ matching (*i.e.*, compensation) networks on both transmitters and receivers. The goal of traditional CPT systems is thus to design efficient matching networks that increase V_{TX} as much as possible [21, 58], even exceeding safe electric field strength levels. Traditional CPT designs arrange the plates as shown in Fig. 3(a), where all the TX plates are in the same plane. Such configurations can minimize the gap between TX and RX plates, thus maximizing the coupling capacitances.

However, besides the 2 capacitors that deliver the power, the 4 plates form 4 parasitic capacitors as shown in Fig. 4. Note that the plates are numbered such that $C_{24} > C_{14}$ and $C_{13} > C_{23}$, *i.e.*, C_{24} and C_{13} are the dominant capacitances for given plate placement, thus the abstract model in Fig. 4 works for all plate placements (Fig. 3). To ease analysis, [58] derived a 3-capacitor equivalent model, which aggregates the 6 capacitors into self-capacitances C_1, C_2, and mutual capacitance C_M:

$$\begin{aligned} C_1 &= C_{12} + (C_{13} + C_{14})(C_{23} + C_{24})/C_S - C_M \\ C_2 &= C_{34} + (C_{13} + C_{23})(C_{14} + C_{24})/C_S - C_M \\ C_M &= (C_{24}C_{13} - C_{14}C_{23})/C_S \end{aligned} \tag{1}$$

where $C_S = C_{13} + C_{14} + C_{23} + C_{24}$. From the 3-capacitor model shown in Fig. 4 we can see that C_M *contributes to power transfer by allowing current to flow through the air gap*. Further, the equations show that C_M is a function of all 6 capacitances, and increasing

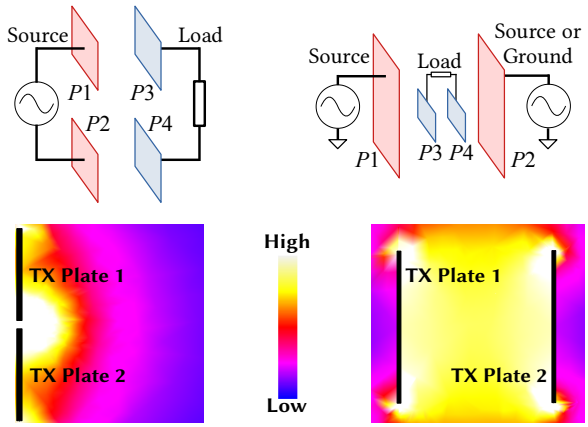

Figure 3: Architecture & ANSYS electric field simulation for (a) conventional CPT, and (b) Capttery.

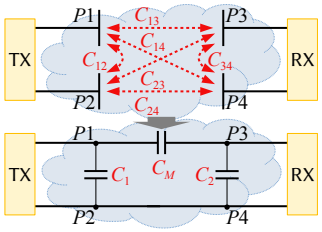

Figure 4: Capacitors in CPT and the 3-capacitor model.

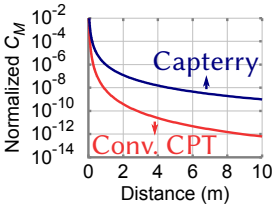

Figure 5: C_M trend vs. distance, higher is better.

C_{14} and C_{23} decreases C_M, negatively impacting power transfer. Meanwhile, the self-capacitances C_1 and C_2 depends on both the TX and RX plates, which *makes V_{TX} sensitive to the environment* as we will show in Sec. 4.

Essentially, a CPT system transfers power through the electric field, as opposed to an inductive power transfer (IPT) system, which conveys energy through the magnetic field. The main advantage of CPT over IPT is that it will not introduce eddy current in metal objects, which makes it potentially more suitable for uncontrolled environments. However, for safety reasons, both FCC and IEEE maintain upper limits of electric field strength for different AC frequencies [24, 27]. For example, at 1 MHz, the maximum permissible exposure for the general public is 614 V_{rms}/m (868 V_{peak}/m), whereas higher frequencies generally result in much more stringent upper limits [27]. The breakdown strength of air is much higher at 3 MV/m [45] and is usually not of concern.

3 CAPTTERY'S ARCHITECTURE

To achieve long-range power delivery, Capttery abandons the traditional CPT architecture. Capttery's new architecture provides power transfer that decreases more slowly as the range increases, by at least an order when compared to the traditional architecture.

To see why we need to depart from conventional CPT architectures shown in Fig. 3(a), we first observe that the co-located TX plates result in the closed electrical field, much like an RF antenna whose emission decreases rapidly as range increases. This fundamentally limits the range of CPT system, and they subsequently can only power receivers millimeters or centimeters away. A survey [20] even concluded that CPT only works at range shorter than IPT!

The failure of the concentrated TX model naturally leads us to a distributed approach, where the 2 TX plates are placed at the 2 opposite ends of the coverage area, as shown in Fig. 3(b). In this case, the electrical field opens up and remains constant between plates, where the RX roams between the TX plates and gets relatively uniform power transfer regardless of distance to any of the TX plates. However, since the TX plates are separated by meters, they have to be driven separately and synchronized to be 180° out of phase for maximum field strength. Alternatively, we can simply drive one side and leave the other grounded. For the rest of the paper, we refer to the driven plate as the active plate.

In order to determine how such configurations would scale, we quantitatively analyze the trend for C_M as range increases. Denote the distance between plate a and b as d_{ab} ($a, b \in \{1, 2, 3, 4\}$ for plates $\{P1, P2, P3, P4\}$), and their area as A_a and A_b, we have the capacitance of the parallel-plate capacitor as $C_{ab} \propto A_a A_b / d_{ab}$. For both conventional or Capttery's cases, we have:

$$C_M \propto \frac{A_2 A_4}{d_{24}} \frac{A_1 A_3}{d_{13}} - \frac{A_1 A_4}{d_{14}} \frac{A_2 A_3}{d_{23}} = \frac{d_{14} d_{23} - d_{24} d_{13}}{d_{24} d_{13} d_{14} d_{23}} \quad (2)$$

For a perfectly-aligned conventional CPT system, $d_{13} = d_{24}$, while $d_{34} = d_{12} \ll d_{13} = d_{24} < d_{14} = d_{23}$. Thus:

$$C_M \propto \frac{d_{14}^2 - d_{13}^2}{d_{14}^2 d_{13}^2} < \frac{d_{34}^2}{d_{13}^4} \quad (3)$$

On the other hand, for Capttery's case, we have $d_{14} = d_{13} + d_{34}$, $d_{23} = d_{24} + d_{34}$, and the range $d_{12} = d_{13} + d_{24} + d_{34}$. Further, consider that $d_{24} + d_{13} + d_{14} + d_{23} = 2d_{12}$ and hence $d_{24} d_{13} d_{14} d_{23} < (d_{12}/2)^4$, Eq. (2) thus turns into:

$$C_M \propto \frac{d_{34} d_{12}}{d_{24} d_{13} d_{14} d_{23}} > 16 \frac{d_{34}}{d_{12}^3} \quad (4)$$

We then plot the trend of C_M for Capttery and conventional CPT in Fig. 5, with $d_{34} = 10$ cm. It is clear that when range increases, Capttery's C_M reduces significantly more slowly than the one for conventional CPT. Recalling that larger C_M leads to higher power transfer, we conclude that *Capttery's new architecture is much more suitable for long-range power delivery.* Additionally, we observe that the conventional architecture is more suitable for larger RX as C_M grows quadratically with d_{34}. In contrast, *Capttery works well with small d_{34} and is suitable for IoT devices.*

We also observe that the new architecture makes Capttery more robust. In the conventional case, C_M and power transfer reach a maximum only when the plates are properly aligned. Unfortunately, IoT devices tend to have much smaller form-factors than the TX, and are usually deployed at arbitrary locations or are mobile, which precludes such alignment. However, in our new distributed architecture, C_M and power transfer are much less sensitive to alignment. As a result, the new architecture makes Capttery more suitable for compact and mobile IoT receivers.

4 DESIGNING A CAPTTERY TRANSMITTER

After the field distribution is optimized for long range, sufficient voltage difference is needed between the plates to reach the desired field strength. We now discuss how Capttery's transmitter generates such a voltage.

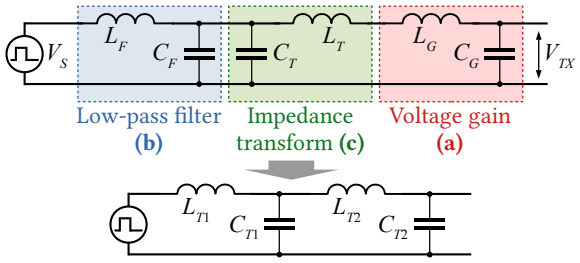

Figure 6: Architecture of the TX matching network.

The design goals for Capttery TX are: ***(i)* extending power delivery range; *(ii)* maximizing power transfer; *(iii)* maintaining safety; *(iv)* supporting multiple RX in a scalable way.** The first two essentially call for **higher TX voltage** V_{TX}, the 3rd goal translates to **full control over** V_{TX}, and the 4th requires the TX to be **invariant of TX-RX coupling**. The latter two requirements are unique to Capttery as previous CPT systems are designed for controlled environments and do not take safety, RX mobility, or multiple RX into consideration. We now analyze how we can achieve these unique goals through TX matching network design.

To generate high V_{TX}, we feed an LC voltage gain stage as shown in Fig. 6(a) with AC voltage V_S at its resonant frequency. At this point, the reactance of L_G and C_G cancels out, allowing a large current to flow through, which subsequently generates a high voltage on C_G due to its reactance. For the same current, lower C_G yields higher V_{TX} as the impedance $Z(C_G) = 1/(j\omega C_G)$, where $\omega = 2\pi f$ and f is the frequency.

However, unlike previous CPT TX, Capttery needs to limit V_{TX} to a certain safe level. We first observe that in ideal conditions, $V_{TX} \to \infty$ if any non-zero V_S at the resonant frequency is applied to the gain stage. This is because at resonance, there is no impedance limiting the current. However, in real L_G and C_G, there will inevitably be non-zero internal resistance. Assume the total resistance is R_G. Then the current flowing through the gain stage would be I_G, which further gives:

$$|V_{TX}| = |I_G Z(C_G)| = \frac{V_S}{2\pi f R_G C_G} \tag{5}$$

Eq. (5) shows that **by manipulating V_S and C_G, we can limit V_{TX} to the desired level**.

Meanwhile, to make the TX invariant of TX-RX coupling, we first observe that C_1 is in parallel with C_G from TX's perspective. This means changes in the TX-RX coupling will detune the TX and cause the voltage to drop unpredictably. Fortunately, since C_1 is usually less than 1 pF in a long-range CPT system, we can make C_G a few tens of pF, so that the contribution of C_1 becomes negligible. This way, the gain stage is always in resonance regardless of C_1 .

The preceding idealized analysis needs a few improvements in practice. For one, a trade-off exists between L_G and C_G values. When operating at resonance, $L_G C_G = 1/\omega^2$. If we choose higher C_G values, L_G becomes smaller, both of which reduce the internal resistances by half for a given Q value[2]. Thus, doubling C_G would approximately halve R_G. However, when C_G doubles, I_G also doubles for the same V_{TX}. The power lost on R_G hence doubles as the power $P_G = I_G^2 R_G$. As a result, smaller C_G achieves higher V_{TX} with less power. We thus choose the smallest C_G that can maintain resonance across different C_M in practice.

Further, V_S will be supplied by a high-efficiency inverter (Sec. 7.1) in the form of square waves. Unfortunately, harmonics in such square waves will waste energy on R_G without contributing to V_{TX}, as the gain stage only resonates at a single frequency. Like previous works [58], we add a 2nd-order 3 dB Chebyshev low-pass filter stage shown in Fig. 6(b). Cut-off frequencies and input impedance set the L_F and C_F values. The input impedance is in turn determined by P_G and V_S. Finally, the output impedance of the filter stage is much higher than the input of the gain stage. We thus add an impedance transforming stage with L_T and C_T in Fig. 6(c).

Together, these stages consolidate into an $LCLC$ network with the following parameters:

$$L_{T1} = L_F \quad C_{T1} = C_F + C_T \quad L_{T2} = L_T + L_G \quad C_{T2} = C_G \tag{6}$$

where L_F, C_F in the filter and L_T, C_T in the impedance transforming stage are computed with existing tools [1, 8].

5 CAPTTERY RECEIVER DESIGN

The goal of Capttery RX is similar to the TX except that it has no safety concerns. To increase range and maximize power transfer, we need to bring the power extraction to its optimum. However, Capttery faces the additional challenge of supporting multiple RX, which requires the power extraction to be invariant to outside coupling. We will first show how to maximize power extraction, and then discuss the invariance in a multiple-RX scenario.

5.1 Maximizing Power Reception

In order to understand how to extract power from the electric field optimally, first recall that a CPT system (Fig. 2) uses a matching network to transform the high over-the-air impedance back to lower impedance that can be used by the load. This network is usually a CL stage as shown in Fig. 7. We treat V_{TX} as a fixed voltage source, as the design in Sec. 4 made it invariant against TX-RX coupling. Such a source is then connected to the RX matching network through the high impedance of C_M. Denote the capacitance in the matching network as C_{RX} (which includes RX plates' self-capacitance C_2 as in Fig. 4), and the inductor as L_{RX}. Finally, the power is delivered into a load R_L. In practice, we need to consider the internal resistance of the inductors and capacitors, hereby denoted as R_{RC} and R_{RL}.

To derive the condition of the requirement for optimal power extraction, we look through the network from R_L's perspective and try to match the complex impedance:

$$\frac{1}{j\omega C_M} \parallel \left(R_{RC} + \frac{1}{j\omega C_{RX}}\right) + (R_{RL} + j\omega L_{RX}) = R_L \tag{7}$$

Note that Capttery needs to satisfy both the real and imaginary parts of this equation for optimal power delivery. Let $\Delta R = R_{RL} - R_L$, we have

$$\begin{aligned} \omega^2(R_{RC}\Delta R C_{RX} C_M + L_{RX} C_{RX}) &= 1 \quad \text{(real)} \\ \omega^2 R_{RC} L_{RX} C_{RX} C_M &= \Delta R C_{RX} + R_{RC} C_{RX} \quad \text{(imaginary)} \end{aligned} \tag{8}$$

To simplify the equations and derive the optimal design, we observe in practice, 10^{-10} F $< C_{RX} < 10^{-12}$ F, $L_{RX} > 10^{-4}$ H, $C_M < 10^{-12}$ F, $R_{RC} < 10^2\ \Omega$, and $|\Delta R| < R_L \approx 10^3\ \Omega$. This means $|R_{RX}\Delta R C_{RX} C_M| \ll L_{RX} C_{RX}$, which makes the former negligible. As a result, the real part reduces to $\omega^2 L_{RX} C_{RX} \approx 1$, indicating that

[2]We use apparent Q, which is the ratio between reactance and resistance. Higher Q leads to higher requirements for inductors and capacitors, and higher frequency sensitivity for resonance.

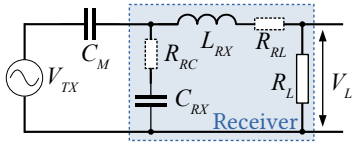

Figure 7: Capttery's receiver.

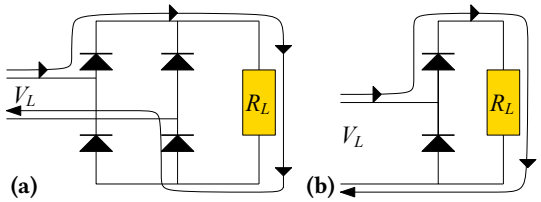

Figure 8: RX rectifiers: (a) full-wave, (b) half-wave.

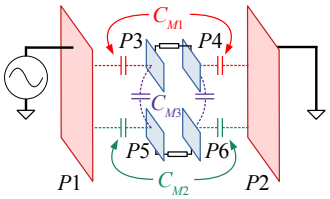

Figure 9: The 2 RX case.

RX matching network should operate at resonance, much like the TX voltage gain stage. By applying such a condition to the imaginary part, we get $\Delta R C_{RX} + R_{RC} C_{RX} \approx R_{RC} C_M$. One solution to satisfy this is to make $\Delta R = 0$ (*i.e.* $R_L = R_{RL}$) and $C_{RX} = C_M$. However, in reality, C_{RX} must be greater than the plate's self-capacitance C_2, and we find $C_2 \gg C_M$, and the optimal load becomes $R_L \approx R_{RC}(C_{RX} - C_M)/C_{RX} + R_{RL} \approx R_{RC} + R_{RL}$, *i.e., the optimal load equals the total internal resistance of the LC loop.*

Eventually, for IoT devices, Capttery needs to convert the high-frequency AC power into DC with a rectifier, whose efficiency will also impact power extraction. There are two options for the rectifier: full-wave and half-wave, as shown in Fig. 8. For the full-wave rectifier, two diodes conduct in series during either half of the cycle, whereas in the half-wave case each diode conducts for a half cycle. As diodes need non-zero forward voltage V_F to turn on, they will consume power. However, the relationship between V_F and current is non-linear, which makes close-formed analysis difficult. The energy storage in the RX matching network further complicates the issue. We hence use simulation and experiments to determine which option is better. From our results, half-wave rectification provides around twice the output voltage (4 times the power) across a wide range of loads. Hence, Capttery employs half-wave rectifiers for the receivers.

In practice, Capttery receivers may be mobile, which essentially requires them to maintain optimal power extraction over varying C_M. Fortunately, the preceding analysis already showed that all terms related to C_M are negligible as $C_{RX} \geqslant C_2 \gg C_M$. We hence conclude that Capttery's RX is inherently invariant across different environments.

5.2 Multiple Receivers in Capttery

To support simultaneous operation of multiple RX, Capttery's receiver should maintain power extraction in the presence of other receivers. From previous sections, we know Capttery RX is invariant against the TX-RX coupling. However, as multiple receivers create C_{M3} between plates of different RX (in addition to the C_{M1} and C_{M2} between TX and the 2 RX, as shown in Fig. 9), Capttery RX must be invariant against such new RX-RX coupling. We will show that *the coupling between RX-RX is weaker than the TX-RX coupling and thus negligible, as long as the receivers are not densely co-located.* We then verify through simulation that the presence of the multiple RX does not decrease the amount of available power in the first place.

We first observe that RX-RX coupling via C_{M3} would be much weaker than the TX-RX coupling. Although the distance between RXs can be much smaller than the TX-RX distance, their size and plate area are also much smaller. More importantly, the voltage across the RX plates would be a fraction of V_{TX}, as RX only taps a small voltage from the electrical field. As a result, we expect the coupling between different RX to be negligible as well unless they come extremely close and C_{M3} becomes large due to extremely short distances.

However, another question arises: would the multiple RX need to share the available power? To understand this issue, we run a simulation with 2 RX, where 1 RX is fixed at the center and the second moves around the entire horizontal plane. We then subtract the power transferred to the fixed RX from the value when it was alone. Our simulation results show that contrary to common intuition that very close receivers can hamper performance, *in the multiple RX case the power transfer to individual RX increases.* The power gain, in general, doesn't follow a particular trend. However, as it always increases power transfer, we conclude that Capttery allows adding RX in a plug-and-play manner without harming power transfer.

Note that Capttery does not break the law of physics — energy is still conserved in the case of multiple RX. The coupling between TX and RX will introduce additional current in the TX's voltage gain stage (Sec. 4) via C_M. However, this current is small when compared to the current ordinarily present inside the stage (as $C_G \gg C_M$) and does not affect its operation. In the case of a vast number of RX, however, such current will eventually sum up and require the TX to automatically adapt for more power, which we leave for future work.

6 ACCURATE POWER MEASUREMENT

Before we get to experimental evaluation, we need to point out one caveat: unlike power measurement in short-range wireless power transfer systems, such measurement in long-range CPT can be deceptive and make the power appear much higher than it really is! The reason is that measurement instruments can create side paths that have much lower impedance than the C_M, and make the power transfer appear to be orders of magnitude higher than its actual value.

To see why this happens, we discuss the following three situations. Fig. 10(a) depicts the first situation, *i.e.*, straight-forward single-ended measurement. Here the probe of an instrument (*e.g.*, oscilloscope) is directly connected to the load. However, the reference point also needs to be connected, which grounds the load, introduces a direct path from the TX to the RX via ground, and inevitably increases the power transfer beyond its true value. To avoid such ground connection, Fig. 10(b) shows a differential measurement scheme, where the probe measures the voltage of both terminals of the load *w.r.t.* ground. Unfortunately, the input capacitance of the probe (to the ground) again creates additional paths. For example, the high impedance oscilloscope probe we use [5] has 15 pF input capacitance, which, albeit being extremely small,

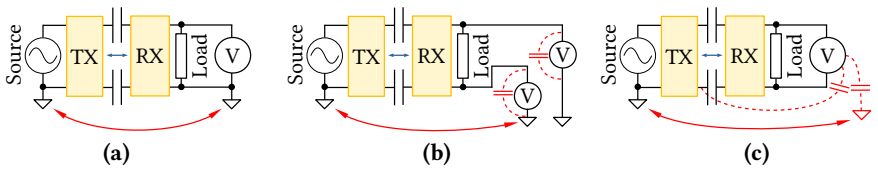

Figure 10: Side paths causing deceptive power measurements: (a) single-ended measurement, (b) differential measurement, and (c) floating measurement.

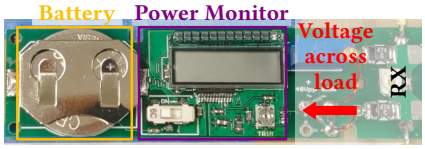

Figure 11: Small-form-factor power monitor for Capttery evaluation.

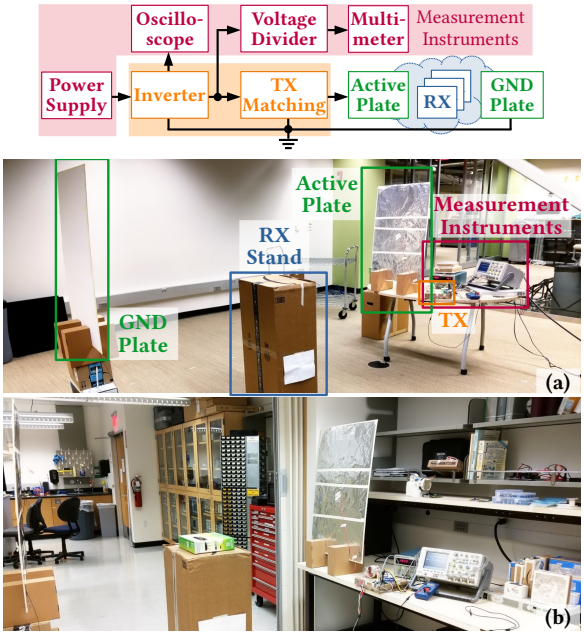

Figure 12: Overview and photo of evaluation setup in (a) room for long-range experiments, and (b) the lab.

is an order of magnitude larger than C_M. Thus, power from this side path completely masks the real power transfer. The last case in Fig. 10(c) shows floating measurement, where an instrument such as multimeter is connected to the load without grounding itself. However, the size of such instruments is usually large, which effectively adds a third RX plate and once again increases power transfer.

To obtain the actual power transfer, we designed a small-form-factor power monitor (Fig. 11) to measure the load voltage. Prior to use, we calibrate its voltage measurements against a multimeter [2]. During experiments, it displays the voltage V_L across a known load R_L in the RX. Then, the power delivered can be computed as $P_L = V_L^2/R_L$. As the monitor has to work regardless of power transfer, we power it with a coin cell battery. The monitor has an area much smaller than the RX plates and will not affect power transfer significantly. Further, the same PCB has both a receiver and the power meter bundled together.

7 IMPLEMENTATION

To evaluate the performance of long-range CPT in real environments, we implemented an end-to-end test setup as shown in Fig. 12. The room in Fig. 12(a) has more space and is used for long-range experiments, whereas the lab in Fig. 12(b) is crowded with metal objects and is used for all other experiments[3]. We now introduce each block of the setup.

7.1 Transmitter

Our transmitter consists of a high-frequency half-bridge inverter, an *LCLC* matching network, and 2 transmitter plates. The inverter takes DC power from a supply [10] and converts it to a square wave. Inside the inverter, a microcontroller (MCU) outputs the desired frequency to the half-bridge drivers, which drive 2 high-speed MOSFET switches to supply the matching network with a square wave of around 1 MHz. Note that unlike full-bridge inverters, the half-bridge inverter's output has a DC component which the *LCLC* matching network will block. In practice, errors in the component values of the matching network and stray capacitances in the environment will make the resonance frequency deviate from the designed value. Considering the high Q-factor of the resonant loop, the frequency should be tunable in steps of a few kHz. To do this, the MCU divides its internal 48-MHz oscillator with a timer to generate a variety of frequencies. However, the divisor must be an integer, which limits the resolution to ~20 kHz. We thus use software to trim the oscillator directly, which has a granularity of ~67 kHz [50] and translates to a ~1.4 kHz step when divided to 1 MHz. As the trimming range is limited, we combine it with the timer. This allows the inverter to cover 600 kHz – 1.4 MHz range with better than 2 kHz resolution.

For the *LCLC* matching network (Fig. 6), we first design the parameters according to Sec. 4. To achieve reasonable power consumption while making the transmitter invariant of environmental changes, we set C_{T2} to 50 pF, which should generate 3 kV at 1 A current. The capacitor is implemented by putting 2, 3-kV 100 pF low-temperature-coefficient capacitors in series. Consequently, L_{T2} is around 500 µH. For stability across temperature and current density, we build L_{T1} and L_{T2} as air-core inductors. Tests on an LCR meter [6] shows that L_{T2}'s Q value is around 120; hence the resistance R_{LC} is ~26 Ω. Accordingly, we target our matching network for $P_G = 30$ W at $V_S = 30$ V, which gives $L_{T1} = 10.2$ µH, $C_{T_1} = 4.15$ nF, and $L_{T2} = 475$ µH. Later in the experiments, we found that the lab environment imposes a stray capacitance of around 60 pF to the plates, which remains stable as long as the transmitter is not moved. We hence reduced L_{T2} to 240 µH. We subsequently ran simulations to find out minimum voltage ratings for each component. It turns out that voltage over C_{T1} is around 90 V. We thus use capacitors rated at 200 V to form C_{T1}. The actual components have value $L_{T1} = 10.3$ µH, $C_{T_1} = 4.3$ nF, $L_{T2} = 238$ µH, and $C_{T2} = 52.3$ pF due to unavoidable error. The whole TX is shown in Fig. 13.

Finally, we use 2 plastic poster boards of 60 cm × 90 cm size covered by heavy-duty aluminum kitchen foil as the transmitter

[3] As Sec. 8.1 will show, such crowded space (which potentially mimics some living environments) may degrade Capttery's performance.

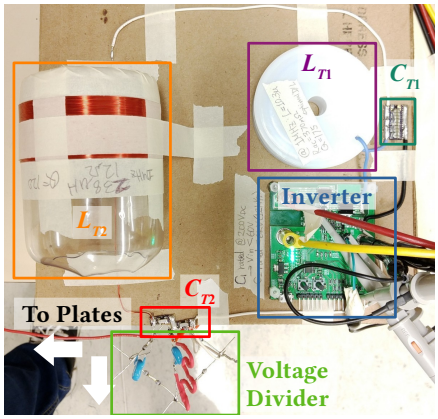

Figure 13: Capttery TX prototype.

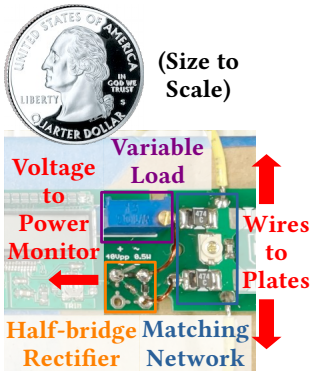

Figure 14: Capttery RX prototype.

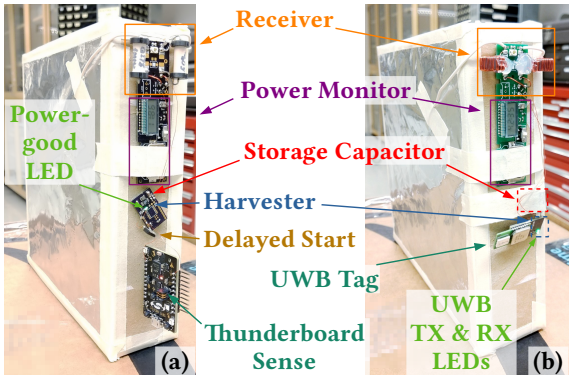

Figure 15: Prototype showcase applications: (a) BLE sensing station; (b) UWB ranging tag.

plates. The plates are mounted vertically with the 60 cm side being horizontal. The output of the TX matching network is feed to the center of the plate through a 22AWG multi-stranded wire taped on the plate. Our experiments show that the location of the feed point does not affect power transfer significantly.

To measure the output voltage V_{TX}, we build a full-wave rectifier with 8 1-kV diodes. We put 2 of them in series for each arm of the rectifier[4]. The output is then divided by 1000× with resistors. We did not directly use a resistor divider on the AC input as at 1 MHz the parasitics of practical resistors severely distort the voltage division. At runtime, we use a multimeter [2] to measure the divided V_{TX}.

7.2 Receiver

Our receivers (Fig. 14) consist of plates, a matching network, a rectifier, and the load.

Kitchen foil and cardboard boxes of various sizes are used to construct receiver plates. In Sec. 8, we denote the box size in the form of $L \times W \times H$, where $L \geqslant W$ and H is the separation between the plates. For our receiver sizes the self-capacitance C_2 (Fig. 4) is in the range of 1 – 10 pF as measured on [6].

On the other hand, we connect 2 inductors to each plate, so that the circuit is fully symmetric and the inductance is doubled. In this way, the RX should always have the same reception when flipped around, and the doubled inductance allows us to use smaller inductors. We use a few different inductors in the receiver matching network to explore the impact of different inductance and Q factors. Some of them are commercial inductors, and others are made in-house with ferrite cores. We measured their parameters at 1 MHz with [6] and summarized them in Table 1. In addition to the plates' self-capacitance, we use a combination of fixed capacitors and trimmers to provide capacitance. The trimmer allows the receiver to adjust to different frequencies and compensate for component errors when the receiver circuits are connected to different sets of plates.

We further use 2 Schottky diodes to form half-wave rectifiers. Finally, the rectifier output is connected to a 1/2 W variable resistor, which acts as the load. The resistor is adjusted to the desired value R_L, verified with a multimeter [2] before each experiment.

[4]At runtime, we found each diode withstood ~1.45 kV voltage, which limits V_{TX} to 2.89 kV.

Table 1: Inductor parameters.

#	Model	Winding Wire/ Approx. # of Turns	Inductance (μH)	Q	Form-factor
1	Murata 82474C	Factory	475	47	Surface Mount
2	Bourns 9250A-474RC	Factory	469	106	Small Axial
3	Bourns 9250A-105RC	Factory	992	96	Small Axial
4	Core of Bourns 5900	38AWG/130	620	180	Large Axial
5	Core of Bourns 5900	40AWG/160	1030	160	Large Axial
6	Ferronics 11-261-K	30AWG/60	333	150	Toroid
7	Ferronics 11-261-K	30AWG/72	478	150	Toroid

7.3 Showcase Applications

We build two showcase applications to demonstrate the potential of mW-level wireless power. The first is a Bluetooth Low-energy (BLE) sensing station. It is based on the Thunderboard Sense, which offers motion, ambient light, ultraviolet, temperature, relative humidity, and barometric sensors. Besides, it features an analog microphone, whose output is amplified and processed on-board to form a single ambient noise level number. The results are sent via BLE to the *unmodified* Thunderboard Sense Android App running on a *commercial off-the-shelf* smartphone. We enabled the low-power mode in the firmware, which disables the gas sensor and RGB LEDs. Further, we connected the power input to an energy harvester whose output is set to 2.5 V. The harvester has a 33 μF storage capacitor, which is insufficient for the start-up process of the Thunderboard Sense, despite that after starting up the power consumption is merely ~2 mW (measured with [9]). We hence added a delayed start circuit with an 82 kΩ resistor and a 2.2 μF capacitor. The delayed start circuit takes the power-good signal from the harvester and turns on a MOSFET switch only after enough charge has been collected.

The other application is an ultra-wideband (UWB) ranging/localization tag. We pack a commercial UWB module (requires 3.3 V), an ultra-low-power MCU, and an energy harvester on a tiny PCB. The MCU runs the ranging protocol at 16 MHz CPU speed and down-clocks to 131 kHz during inactive periods. We ported the `TREK1000` [12] firmware to the MCU, and it works with *unmodified* `TREK1000` anchors. The channel and bit rate are hard-coded to 2 and 6.8 Mbps, respectively. We further modify the firmware such that it wakes up the tag only when the harvester asserts the power-good signal. When power is sufficient, the tag does 2-way ranging with 3 or 4 anchors at 10 Hz rate, and the power consumption is ~5 mW measured by [9]. Since the tag has a peak power consumption of over 440 mW, we use a relatively large storage capacitor of 330 μF.

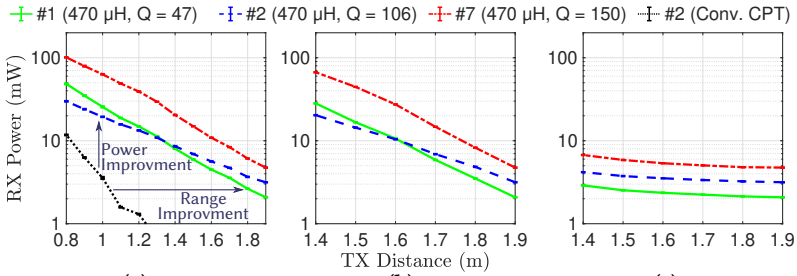

Figure 16: Power vs. distance under fixed V_{TX}: (a) move both plates; (b) move active plate; (c) move ground plate.

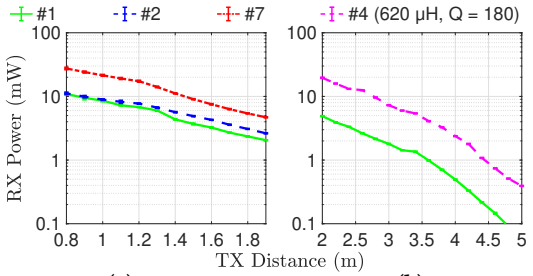

Figure 17: Power vs. distance under fixed field strength, for (a) short and (b) long distances.

8 EVALUATION

In this section, we first evaluate the performance of Capttery under various conditions through single-receiver experiments. We then explore the interaction/interference between receivers. Finally, we demonstrate the performance of the showcase applications.

Our major findings are as follows:

- Capttery can deliver 1 – 10 mW of power wirelessly while conforming to the safety limit, with plates as small as 5 cm × 6 cm, and for a range up to 4.4 m;
- Capttery allows adding receivers in a plug-and-play manner without a significant decrease in power transfer, and with 10 RX it can deliver a total of 26.5 mW at 1.9 m distance;
- Capttery is able to power real-world computation and communication loads with *standard* protocols.

Unless otherwise noted, the experiments were conducted in the lab shown in Fig. 12(b) and the following parameters were used: electrical field strength of around 600 V_{rms}/m (850 V_{peak}/1.7 $kV_{P\text{-}P}$), which translates to 1.615 kV_{peak} at 1.9 m distance between TX plates; the receivers are centered between the 2 TX plates; the lower edges of the TX plates are 0.86 m off the ground; and the stand for RX is 1.09 m in height. The RX circuits are placed next to the gap of the 2 RX plates, much like the showcase scenarios in Fig. 15. We define the horizontal direction perpendicular to the plates as the axial direction, and the horizontal direction parallel to the plates as the lateral direction. For each measurement, we take 5 readings and plot the standard deviation as error bars (which are usually insignificant).

8.1 Profiling a Single Capttery Receiver

Range.

We first evaluate how distance affects the power transfer under fixed V_{TX} = 1.6 kV_{peak}. We consider three different cases: the distance between the RX and both TX plates are varied symmetrically, only the active TX plate is moved, and only the ground TX plate is moved. For each case, we try 3 receivers with inductors #1, #2, and #7 (see Table 1), all of which are around 470 μH, and the loads are 1.2 kΩ, 800 Ω, and 800 Ω, respectively. All the receivers use 16 × 16 × 4 cm plates. Also, Fig. 16(a) includes the conventional CPT case, where the collocated TX plates are separated by 0.7 m, while the RX plates are separated by 10 cm (edge-to-edge). Note that for this configuration, larger separation within TX/RX plates leads to higher power transfer (Sec. 3). Fig. 16(a) clearly shows that at long distances, Capttery's architecture provides much higher power transfer than the conventional one. We also see that power transfer increases as distance shortens, which is expected. However, from Fig. 16(b) and (c) we notice one interesting trend: the ground plate does not affect power transfer nearly as much as the active plate. *We hypothesize that this is due to grounded metal objects around the setup.* On the one hand, they will prevent the electric field from being constant between TX plates; on the other hand, they also couple with the RX and decrease the dependency on the ground plate.

We then keep the average field strength constant at the human-safe 600 V_{rms}/m (850 V_{peak}) level for short and long distances. Wall-plug power taken by TX ranges from 0.9 W at 0.8 m to 12.7 W at distances greater than 3.4 m, at which point the TX reaches its maximum voltage of 2.89 kV_{peak} limited by rectifiers in the measurement circuit. The long-range experiment is conducted in an empty and more spacious room as shown in Fig. 12(a), where no metal objects are present to provide additional ground plates. The TX plates are 0.88 m above the ground, whereas RX is at 1.01 m height. For the long-distance experiment, we use two different receivers: one uses high-Q inductor #4, 800 Ω load, and 20×20×5 cm plates; the other uses inductor #1 with lower Q, 1.2 kΩ load, and 16 × 16 × 4 cm plates (the same as short-distance). In the short-distance setup, we see RX with inductor #1 has power ~2 mW at 1.9 m distance, as shown in Fig. 16(a), but in the empty room, Fig. 17 shows that power transfer at 2 m distance is ~5 mW. This suggests that our hypothesis is correct. Note that stray ground coupling does not generate heat as opposed to the case of IPT, even if the object is close to the TX. However, the building's structure inevitably contains grounded steel structures, which shunt the electric field and shorten the power transfer range. In our long-range experiment shown in Fig. 17(b), the high-Q, large-plate RX can get over 1 mW power for up to 4.4 m, while the low-Q, small-plate RX gets below 1 mW before reaching 3.6 m. Further, we replicate the setup in ANSYS simulations for a distance of up to 10 m. Our results show that the power transfer is above 1 mW for up to 5.5 m, and reduces to 0.3 mW at 10 m, which matches our experiments. Overall, *Capttery delivers mW-level power with a range of up to 4.4 m.*

Impact of RX Location.

To understand the coverage of Capttery, we keep the TX plates fixed and move the RX away from the center point on either the axial or lateral axis. The RX uses inductor #4 and 16 × 16 × 4 cm plates. Fig. 18 shows that power transfer increases sharply as the RX approaches the active plate, which again indicates stray ground coupling. Meanwhile, the power transfer along the lateral direction is slightly asymmetrical. The TX plate is close to a wall with metal

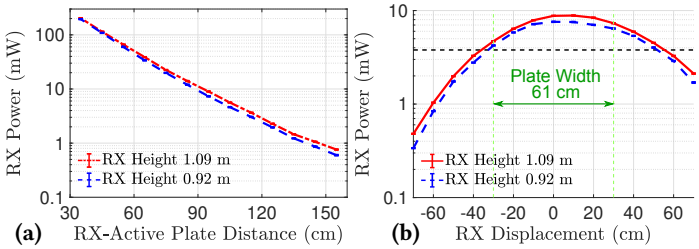

Figure 18: Spatial coverage: (a) axial displacement; (b) lateral displacement.

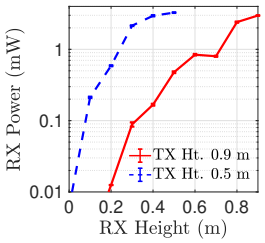

Figure 19: Impact of RX height.

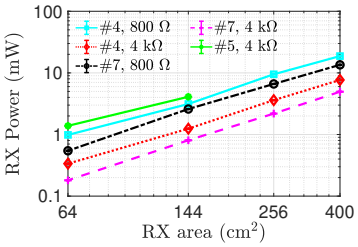

Figure 20: Impact of RX area.

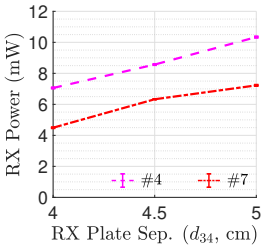

Figure 21: Impact of RX plate separation.

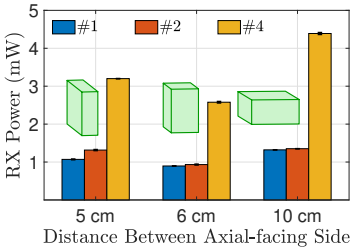

Figure 22: Effect of plate arrangement for fixed RX volume.

objects on the left side, as shown by Fig. 12(b), which may have lowered the power transfer on the left side. We also notice height does not change the trend, but at 0.92 m height, the RX is facing the lower edge of the TX plates and the power drops slightly.

Note that although the plate width is 24 inches or 60 cm, the half-power range on the lateral direction is around 80 cm, and over a 1.3 m range the power delivered is more than 1 mW. This means *the coverage of Capttery extends well beyond the area covered by the TX plates*, and it does not need to wrap the whole room in metal as in [18].

Meanwhile, we also vary the height of the RX (with inductor #2 and the same plates), where TX's lower edge is 0.9 m above the floor. We then lowered the TX to 0.5 m and repeated the experiments. Results in Fig. 19 show similar trends to the lateral case. However, after the TX is lowered by 0.4 m, the 10 µW point is only lowered by ~0.2 m, which indicates that the floor may have distorted the electric field. Nevertheless, with a TX-to-floor distance of 0.5 m, milliwatt power transfer can be achieved 25 cm above the floor.

Impact of RX Plate Size and Separation.

To see how the size of the RX affects its power reception, we test power transfer with square RX plates of different area and separation. We first take a $20 \times 20 \times 5$ cm RX and trim it down. Note that smaller area yields lower self-capacitance, which means a larger inductance can be used. For all areas, we use inductor #4 and #7 with 800 Ω load. Inductor #5 only works with smaller plates and is tested with 4 kΩ load. It has the highest inductance but lowest Q among the three. From Fig. 20 we see that the *power transfer grows linearly with RX plate area* (note both axes are logarithmic). Since C_M increases linearly with the area as well, this suggests that *power transfer increases linearly with* C_M. With lower areas we have lower power transfer, *but also higher inductance, which compensates the power transfer loss to some degree.* Although the trend shows that tiny devices at millimeter-scale may not get milliwatt power transfer, *with a small area of 30 cm^2 Capttery can still provide milliwatts of power with the help of higher inductance.* We believe that Capttery RX can be made reasonably small (a few cm^3) with proper design.

Meanwhile, Sec. 3 indicates that C_M and thus power transfer should increase with the distance between RX plates. We use 3 different boxes with 16×16 cm plates, separated by 4/4.5/5 cm. Results in Fig. 21 show that *power transfer indeed increases with RX plate separation.*

Finally, to explore how to arrange RX plates on a fixed volume, we take a small box of $10 \times 6 \times 5$ cm (300 cm^3) size and use 3 different opposing faces as RX plates, *i.e.*, put the 5-cm, 6-cm, and the 10-cm side along the axial direction. We use inductor #1 (2 in series for each plate) with 1.4 kΩ load, and inductor #3 and #5 with 800 Ω load. In every case, the inductance sums up to about 2 mH. Fig. 22 shows that the power transfer is somewhat similar for the same inductor, and does not increase monotonically when the longer side is in the axial direction. Since C_M increases linearly with both area and plate separation, this trend may vary depending on the exact geometry of the RX. Nevertheless, these results suggest that *Capttery's power transfer is relatively insensitive to the way that RX plates are placed.*

Impact of Orientation.

We hypothesize that the RX will get no power transfer when it is parallel to the electric field, as the potential on the 2 plates would be equal. To verify this, we rotate one RX ($16 \times 16 \times 4$ cm, inductor #4, 8 kΩload) around its vertical center axis, where 0° refers to the direction parallel to the TX plates. From Fig. 23 we can see that the power indeed goes to 0 when the RX plates are perpendicular to the TX plates. The pattern roughly follows the shape of the cosine function, which suggests that the power transfer can be approximated by defining an effective RX cross-section $A'_{RX} = A_{RX} \cos\theta$, where θ is the angle from the normal position and A_{RX} is the receiver area.

This kind of sensitivity towards angle creates a blind zone for CPT. However, the problem can be solved in 2 ways: by adding patches of plates on all six surfaces of a cubic RX and then using multiple receiver networks like a multi-phase transmission line system, or by having multiple orthogonal TX which operate in a multiplexed fashion. The total power received should become more stable across different orientations. We leave such design for future exploration.

Robustness.

To test the robustness of our system against user interaction (*e.g.* touch and blocking), we walk across the area between TX and RX, then blocked/touched RX plates ($16 \times 16 \times 4$ cm RX, inductor #4) with our hands. For the safety of the tester, we lowered V_{TX} to 800 V, which corresponds to ~300 V_{rms}/m. In Fig. 24, "Normal" is the

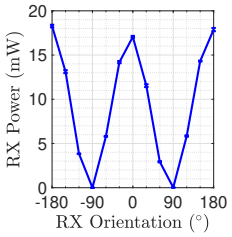

Figure 23: Impact of orientation.

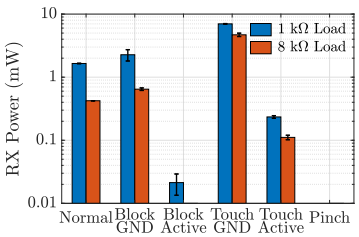

Figure 24: Effect of human blockage & touching (reduced V_{TX}).

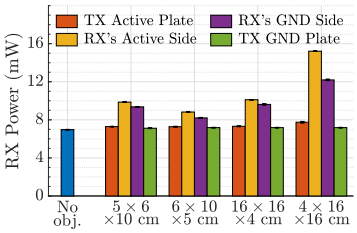

Figure 25: Effect of metal objects (size in vert.×lat.×ax.).

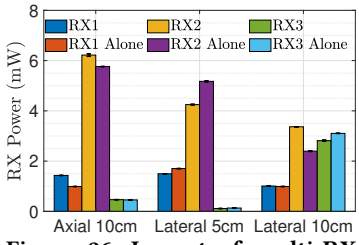

Figure 26: Impact of multi-RX distribution.

case without disturbance, while in "Block GND/Active" the tester stands between the RX and grounded/active TX plates, respectively. In "Touch GND/Active", the tester touches the RX plate facing the grounded/active TX plates, respectively, while in "Pinch", the tester holds the RX by touching both RX plates with the same hand. From Fig. 24 we can see that *blocking the active TX plate causes the power transfer to decrease while blocking the grounded side generates extra ground coupling and increases power transfer.* However, *pinching (thus shunting) the RX causes power transfer to diminish.* We also hold the RX by hand instead of putting it on the stand shown in Fig. 12. When we stand between the RX and the grounded TX plate, power transfer increases by over 70%. However, when we stand between the RX and the active TX plate, power transfer drops by nearly 80%, which follows the trends of cases (b) and (c) in Fig. 24. Hence, making Capttery more robust still poses a challenge for future work (Sec. 10).

In addition, we characterize the effects of metal objects by placing different boxes wrapped in aluminum foil, with the same plates and inductor #2 under normal V_{TX}. From Fig. 25 we can see that these metal objects have negligible effects when placed near the TX plates and cause an increase in power transfer when placed near the RX, as long as they do not shunt the RX. In the case where the metal object shunts the RX, it can be expected that the power transfer would diminish like the case (h) in Fig. 24.

8.2 Multi-RX Performance

Impact of Spatial Distribution.

To understand the interaction between different receivers, we first put 3 RXs together in simple configurations, spreading them out along either the axial or lateral direction. All the RXs use inductor #1 and 16×16×4 cm plates. Fig. 26 indicates that when the receivers are put together in the axial direction, power transfer to each receiver actually increases. This trend matches our ANSYS simulation, where we try up to 5 RXs with different spacing. We hypothesize that this results from the reduced effective distance between the TX and RX, as there are more and more metal plates between them. Meanwhile, when RXs are put together in the lateral direction in close proximity, their power transfer will slightly decrease. After we increase the spacing, however, some of the RXs again see increased power. Overall, *the presence of multiple RXs does not harm power transfer significantly.*

Heterogeneous Receivers.

We further tightly pack 10 RXs in a 51 cm × 38 cm space as shown in Fig. 27. The tight spacing ensures that the RXs interfere with each other more than in the normal use cases. These receivers have different inductors and plates sizes as shown in Table 2. We can

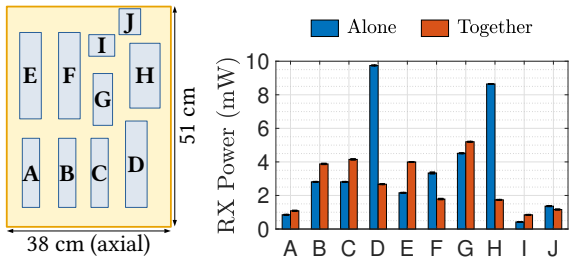

Figure 27: Layout and power transfer of 10 RX.

Table 2: Receivers in Fig. 27.

#	Plate Size (cm)	Inductor	Load (Ω)	#	Plate Size (cm)	Inductor	Load (Ω)
A	16 × 16 × 4	#1	1200	F	20 × 20 × 5	#1	1200
B	16 × 16 × 4	#7	800	G	20 × 12 × 4.5	#4	800
C	16 × 16 × 4	#2	800	H	22 × 15 × 7	#2	800
D	20 × 20 × 5	#1	1200	I	10 × 6 × 5	#3	1000
E	20 × 20 × 5	#1	1200	J	10 × 5 × 6	#5	1000

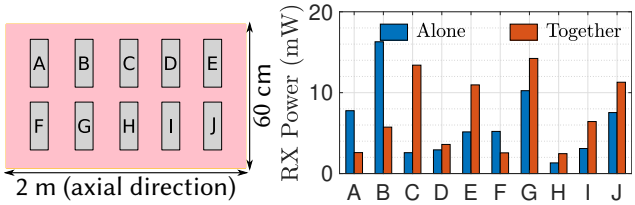

Figure 28: Layout and simulated power transfer for 10 RX.

see that depending on location and receiver characteristics, they demonstrate different trends. However, nearly all of them have power transfer greater than 1 mW when put together. We also run a series of ANSYS simulations with RXs of different characteristics evenly spaced out over a larger space, as shown in Fig. 28. We found that when the spacing between the RXs is less than the scale of the RX, the power transfer tends to decrease, while the power transfer is likely to increase when the receivers are spaced further apart. This matches our observation in Sec. 5.2, where RX remains tuned until C_1 becomes comparable to RX's self-capacitance. Thus, we conclude that with a moderate number of IoT devices in similar sizes, RX can be added in a plug-and-play manner without negatively affecting each other, as long as the spacing is larger than the device size.

8.3 Showcase Applications

To show how Capttery would benefit real-world applications, we connect our RX with a BLE sensing station and a UWB ranging tag[5]. We then profile the power reception and performance. In both cases, we use 20 × 20 × 5 cm plates. The distance between TX plates remains 1.9 m, but as power transfer increases when RX moves

[5]Video for the UWB ranging tag can be found at https://youtu.be/TW976W7BOLU.

toward the active TX plate (Sec. 8.1), we move our showcase setup in that direction until it starts up.

BLE Sensing Station.

The BLE sensing station runs stock firmware that is not harvester-aware. As a result, its startup process is energy-intensive. We had to move the RX to within 0.7 m of the active plate before it started working. However, once started up, the harvester is able to collect nearly 12 V voltage on its storage capacitor regardless of workload, as the average power consumption is much lower. The readings from the sensors are reliably updated roughly once every 2 seconds in the App. This demonstrates that our system can support both standard BLE communication and simple signal processing for computing sensor values (Sec. 7).

UWB Ranging Tag.

The RX for the UWB tag uses inductor #7. Thanks to our harvester-aware firmware, the system starts easily more than 1 m away from the active plate. However, the ranging update rate will vary depending on the power received. The wirelessly-powered tag reaches its full 10 Hz update rate at 0.89 m away from the active plate, where it would consume about 5 mW on average. As the location moves away from the active plate, ranging frequency and collected voltage decrease. Eventually, at 1.04 m the harvester cannot collect enough energy to restart the tag. Considering that some IoT Wi-Fi solutions have power consumption similar to UWB, our system should also be able to power standard Wi-Fi communication.

9 RELATED WORKS

Capttery presents the first human-safe continuous milliwatt-level power transfer at multiple meters of distance, enabling smart and intelligent devices. Capttery's CPT approach is compared with other technologies in Table 3. We briefly discuss each of the technologies listed in the table.

Inductive Power Transfer (IPT).

IPT uses one or multiple coils to transfer power through magnetic fields [34]. Recent works on IPT [3, 30, 40] and industry standards [57] are evolving for better performance. However, IPT inherently suffers from the presence of conductors in the air gap due to eddy currents [23], which reduce power transfer and cause unexpected heating [37]. Despite years of research, the latest commercial IPT systems still suffer from the problem [51]. Besides, the range of IPT is still less than a meter. Therefore, IPT is extensively used by smartphones, toothbrushes, and other devices that can be placed in proximity to the charger [13]. In general, IPT has a limited range proportional to the coil's diameter due to the closed nature of magnetic fields. Capttery's fundamental advantage over IPT is that electric fields are open in nature and therefore can provide a longer range.

Quasistatic Cavity Resonance (QSCR).

QSCR works by creating quasi-static magnetic fields within a room, which is enclosed by a metal cage, to transfer power wirelessly to all receiving devices within that cavity [17, 18]. QSCR works in near-field instead of far-field by creating standing waves that fill the resonant cavity with a uniform strength [16, 47]. This method achieves much longer distance than traditional IPT and is generally human-safe. Unfortunately, like IPT, QSCR also carries energy through oscillating magnetic fields, which cause eddy current losses [18, 25]. Nevertheless, such technology can deliver watts of power over meters of distance for rooms with metallic walls and ceilings. However, these requirements would preclude outside wireless signals, such as cellular networks. In contrast, Capttery's experimental environment is filled with large metal shelves and instruments with metal casings, some of which are in close proximity to the setup, as shown in 12(b). In addition, Capttery's coverage extends beyond the physical size of the plates, so covering the room with metal is unnecessary.

Far-field RF for Power.

Far-field RF (including RFID) is an appealing candidate for WPT as it can be transmitted and received using the same set of hardware used for wireless communication. Nonetheless, in reality, the power received follows the inverse square law for path loss and is extremely low for IoT applications [33]. Power in human-safe RF [4, 54] typically drops to less than 60 μW at a few centimeters of distance from the transmitter, with an omnidirectional antenna. Also, these power signals interfere with information signals and degrade the capacity of congested WiFi networks [39]; therefore RF power can not be a continuous source of power. To alleviate this issues, in [54], the power beacons are transmitted in silent periods, and different devices have to wait for corresponding times to gather sufficient energy for their intended function. To further extend range, the proposed methods include using relays, high power beacons, and directional antennas [22, 52]. Several startups claim to transfer enough power to charge mobile devices across a typical living room [7, 11], where the RF transmissions exceed FCC safety limitations and are potentially unsafe for humans. In contrast, Capttery is human-safe and provides continuous power transfer of milliwatts that can scale to 10s of devices without any impact on power delivered to any receiver.

Existing Capacitive Power Transfer (CPT).

Before this work, researchers have explored CPT in the electric vehicle (EV) charging scenario [38]. The distances were very short (up to 15 cm), and plate areas were in square meters [36, 37, 58]. As the power involved was in kilowatts, the primary design concern was efficiency, and the field strength was unsafe for humans. Authors in [32] developed a CPT circuit for USB power transfer, but the distance is only 0.13 mm, which is equivalent to wired charging. In [35], authors proposed rotary coupling structures with cylinders and disks, but they are limited to short range as well. In [55], researchers uses 13.56 MHz CPT to power wearable devices. The power delivered is well below 1 mW, and it essentially requires the human body to have contact with one of the plates. Capttery is thus the first CPT system we are aware of to reach meters of range.

Other Wireless Power Transfer Methods.

In [28], authors use a high-intensity laser to wirelessly charge mobile devices, delivering up to 2 W at a range of 12 meters for a receiver with 100 cm^2 area. However, lasers are inherently dangerous as even a 1 μs exposure to a watt-level laser beam is enough to do extensive damage to sensitive eye tissues. Due to this issue, complicated tracking and safeguarding mechanisms are mandatory [28]. Furthermore, the system cannot sidestep blockage issues, and scaling to multiple RX is non-trivial. In [19], an ultrasonically powered implant is proposed. The implant is able to harvest energy

Table 3: Comparison between various wireless power transfer (WPT) systems.

Underlying Tech	Continuous Power Delivery	# Devices	End-to-end Efficiency	Other Inherent Limitations	Special Infrastructure	Showcase Scenario
IPT [30, 34, 48, 57]	1 W total at 0.5 m	6	$<$ 40% at 0.5 m	Metal blockage, eddy current loss	Multiple coils, detectors	Smartphone Charging
RF & RFID [39, 54]	6.3 μW at 6.41 m	Scalable	$<$ 0.001% at 0.5 m	Interference to data communication	High-power RF, high gain antennas	Battery & supercapacitor charging, Camera, and Temp sensor
Laser [28]	2 W at 4.3 m	1-to-1	10% – 20%	LoS requirement	Laser TX, cooling, intrusion detection	Mobile phone charging
Ultrasonic[19, 44]	1 mW at 0.03 m	Scalable	~0.2% at 0.1 m	Low range and blockage	Ultrasound TX	Oscilloscope reading
Cavity Resonance [16–18, 47]	5 W at 2.5 m	Scalable	20% – 50%	Block outside wireless signal, eddy current loss	Fully-covered metal room, pole	Mobile charging and 5W table fan
CPT (this work)	1 mW at 4.4 m	Scalable	up to 0.74% at 1.9 m	High E-field near grounded metal objects Blocked by shunting	Metal plates, matching networks	BLE sensing station and UWB ranging tag

with up to 10 cm distance, but the power quickly degrades to μW level. Recently, a startup "ubeam" has proposed to charge mobile phones using sound waves, but the company has never shown a fully working prototype [26]. In general, sound waves require unobstructed paths and have high absorption rates in air, and are thus unsuitable for long-range power delivery.

Energy Harvesting and Scavenging.

Energy harvesting and scavenging have been a hot topic, which promises to power billions of wireless IoT nodes at little additional cost. Heliomote, a sensor node powered from outdoor solar energy, can harvest at a power density of 15 mW/cm^2 [42]. However, for indoor lighting, this figure quickly falls to tens of μW/cm^2 [43]. AmbiMax is powered by both wind and solar, which can harvest 50 mW on average if a wind speed of 10 m/s is maintained for at least 6 hours per day [41]. An ambient RF powered sensing platform can harvest 60 μW at a range of about 4 km from a VHF or UHF TV tower [46], as the tower typically transmits at multiples of kilowatts. A piezoelectric power generator is designed in [49], which can harvest 108 μW power after applying periodic stress. Similarly, thermoelectric power of 40 μW/cm^3 can be extracted from a heat gradient of 10°C [42]. However, all of these energy sources occur intermittently, which makes them unreliable and difficult to sustain in practice.

10 LIMITATIONS AND FUTURE WORK

Efficiency. The current Capttery implementation lacks efficiency optimization. Most of the energy is wasted in the inductor (L_{T2} in Fig. 6), whose large inductance inevitably leads to tens of ohms of AC resistance, which converts tens of watts into heat while ~1 A resonance current is flowing through it. To improve efficiency, we need to redesign the inductors and explore additional compensation network topologies. Automatic control schemes that reduce overall C_{T2} can also lower the resonant current, and thus reduce wasted power. We leave such optimizations for future work.

Safety concerns. Although Capttery ensures that the field strength does not exceed the safety limit, its active plate does carry high voltage and is unsafe to touch. However, unlike low-frequency or DC current that interferes with nerve function and can be fatal, high AC current at 1 MHz causes heating and damage only in shallow tissue [14]. One way to circumvent the issue is to put insulation over the plate, which does not hinder Capttery's operation. We attached a 3×3 cm^2 square of aluminum foil with a piece of a thin insulator (3 mm) to Capttery's TX plate, and the other end through a human body model [31] to the ground. The peak current is 34 mA, which is perceptible but safe [14]. This current can be further reduced by using thicker insulation. Meanwhile, under certain conditions larger or grounded metal objects could distort the electric field, and can cause the field strength to exceed the designed value in certain places. Future Capttery TX can incorporate sensors and automated control to mitigate these risks. We also note that at 1 MHz, the electric field does not penetrate the human body very well, probably due to skin effects and the shielding of conductive tissue. To verify, we submerged an RX in saline. The RX did not pick up any power, indicating that the in-body electric field would be very weak and is unlikely to affect internal organs. However, understanding the potential long-term health effects of Capttery requires rigorous clinical study in the future.

Making CPT more robust. During our experiment we noticed issues such as stray ground coupling and certain human blockage that reduce power transfer. In addition, with a single set of TX plates, there will be little to no power transfer for specific RX orientations. While this can be partly mitigated by carefully locating the TX plates, eventually Capttery needs fundamental solutions to make it more robust, especially for mobile RX. One of the solutions might be adding MIMO to the transmitter as in [30]. We leave such exploration for future work.

11 CONCLUSION

Despite decades of research, providing continuous power to IoT devices remains a challenge. In this paper, we propose Capttery, which delivers wireless power to multiple IoT devices over a long range. The fundamental intuition behind Capttery is that, with an innovative capacitive power transfer architecture, the electric field can be made invariant over distance. We further design, implement and evaluate a Capttery transmitter and receivers that allow scalable concurrent operation. Together, we achieved mW-level power delivery across the room, which is sufficient for powering communication and computation of IoT devices.

ACKNOWLEDGMENT

We appreciate insightful comments and feedback from our shepherd, Jeremy Gummeson, and the anonymous reviewers. We would like to thank the Communication, Systems and Networking Group and Prof. Xinyu Zhang's Group from UC San Diego for their valuable feedback and comments. We would also like to thank Vincent Leung from UC San Diego for sharing the Circuit Lab.

REFERENCES

[1] Impedance Matching Network Designer. https://home.sandiego.edu/~ekim/e194rfs01/jwmatcher/matcher2.html, 1997.

[2] B&K Precision 2703B Digital Multimeter. https://bkpmedia.s3.amazonaws.com/downloads/manuals/en-us/2703B_manual.pdf, 2001.

[3] WiT-5000 development kit data sheet. WiTricity Corporation, 2015.

[4] P2110B 915 MHz RF Powerharvester® Receiver. http://www.powercastco.com/wp-content/uploads/2016/12/P2110B-Datasheet-Rev-3.pdf, 2016.

[5] 10074C Passive Probe. https://www.keysight.com/en/pd-1000000007%3Aepsg%3Apro-pn-10074C/passive-probe-101-150-mhz-15-m, 2018.

[6] E4980A Precision LCR Meter. https://www.keysight.com/en/pd-715495-pn-E4980A/precision-lcr-meter-20-hz-to-2-mhz, 2018.

[7] Energous. https://www.energous.com/, 2018.

[8] LC Filter Design. https://www-users.cs.york.ac.uk/~fisher/lcfilter/, 2018.

[9] Monsoon Low Voltage Power Monitor. https://www.msoon.com/lvpm-product-documentation, 2018.

[10] N5770A Power Supply. https://www.keysight.com/en/pd-839186-pn-N5770A/power-supply-150v-10a-1500w, 2018.

[11] Ossia Inc. http://www.ossia.com/, 2018.

[12] TREK1000 Evaluation Kit. https://www.decawave.com/product/trek1000-evaluation-kit/, 2018.

[13] Wibotic. https://www.wibotic.com/, 2018.

[14] J. H. Bernhardt. The establishment of frequency dependent limits for electric and magnetic fields and evaluation of indirect effects. *Radiation and Environmental Biophysics*, 27(1):1–27, 1988.

[15] D. Bharadia, K. R. Joshi, M. Kotaru, and S. Katti. Backfi: High throughput wifi backscatter. In *Proceedings of the 2015 ACM Conference on Special Interest Group on Data Communication*, SIGCOMM '15, pages 283–296, New York, NY, USA, 2015. ACM.

[16] M. J. Chabalko and A. P. Sample. Resonant cavity mode enabled wireless power transfer. *Applied Physics Letters*, 105(24):243902, 2014.

[17] M. J. Chabalko and A. P. Sample. Three-Dimensional Charging via Multimode Resonant Cavity Enabled Wireless Power Transfer. *IEEE Transactions on Power Electronics*, 30(11):6163–6173, Nov 2015.

[18] M. J. Chabalko, M. Shahmohammadi, and A. P. Sample. Quasistatic Cavity Resonance for Ubiquitous Wireless Power Transfer. *PLOS ONE*, 12, 2017.

[19] J. Charthad, M. J. Weber, T. C. Chang, and A. Arbabian. A mm-Sized Implantable Medical Device (IMD) With Ultrasonic Power Transfer and a Hybrid Bi-Directional Data Link. *IEEE Journal of Solid-State Circuits*, 50(8):1741–1753, 2015.

[20] J. Dai and D. C. Ludois. A Survey of Wireless Power Transfer and a Critical Comparison of Inductive and Capacitive Coupling for Small Gap Applications. *IEEE Transactions on Power Electronics*, 30(11):6017–6029, 2015.

[21] J. Dai and D. C. Ludois. Wireless electric vehicle charging via capacitive power transfer through a conformal bumper. In *2015 IEEE Applied Power Electronics Conference and Exposition (APEC)*, pages 3307–3313, March 2015.

[22] S. De and R. Singhal. Toward Uninterrupted Operation of Wireless Sensor Networks. *Computer*, 45(9):24–30, 2012.

[23] C. Deqing, W. Lifang, L. Chenling, and G. Yanjie. The power loss analysis for resonant wireless power transfer. In *2014 IEEE Conference and Expo Transportation Electrification Asia-Pacific (ITEC Asia-Pacific)*, pages 1–4, Aug 2014.

[24] FCC. Evaluating Compliance with FCC Guidelines for Human Exposure to Radiofrequency Electromagnetic Fields, 1997.

[25] F. Fiorillo. *Characterization and measurement of magnetic materials*. Elsevier Academic Press, 2004.

[26] L. Gomes. Experts Still Think uBeam Through-the-Air Charging Tech Is Unlikely. *IEEE Spectrum*, 2015.

[27] IEEE. IEEE Standard for Safety Levels with Respect to Human Exposure to Radio Frequency Electromagnetic Fields, 3 kHz to 300 GHz, 2005.

[28] V. Iyer, E. Bayati, R. Nandakumar, A. Majumdar, and S. Gollakota. Charging a Smartphone Across a Room Using Lasers. *Proc. ACM Interact. Mob. Wearable Ubiquitous Technol.*, 1(4), 2018.

[29] V. Iyer, V. Talla, B. Kellogg, S. Gollakota, and J. Smith. Inter-technology backscatter: Towards internet connectivity for implanted devices. In *Proceedings of the 2016 ACM SIGCOMM Conference*, SIGCOMM '16, pages 356–369, New York, NY, USA, 2016. ACM.

[30] J. Jadidian and D. Katabi. Magnetic MIMO: How to Charge Your Phone in Your Pocket. In *Proc. of ACM MobiCom*, 2014.

[31] JEDEC. ESDA Standard for Electrostatic Discharge Sensitivity Test-Human Body Model (HBM) - Component Level. Technical report, 2017.

[32] M. Kline, I. Izyumin, B. Boser, and S. Sanders. Capacitive power transfer for contactless charging. In *Proc. of IEEE APEC*, 2011.

[33] S. Kumar et al. RF energy transfer channel models for sustainable IoT. *IEEE Internet of Things Journal*, 5(4):2817–2828, Aug 2018.

[34] A. Kurs, A. Karalis, R. Moffatt, J. D. Joannopoulos, P. Fisher, and M. Soljačić. Wireless power transfer via strongly coupled magnetic resonances. *Science*, 317(5834):83–86, 2007.

[35] C. Liu, A. P. Hu, and N. C. Nair. Coupling study of a rotary Capacitive Power Transfer system. In *Proc. of IEEE ICIT*, 2009.

[36] F. Lu, H. Zhang, H. Hofmann, and C. Mi. A Double-Sided LCLC-Compensated Capacitive Power Transfer System for Electric Vehicle Charging. *IEEE Transactions on Power Electronics*, 30(11):6011–6014, 2015.

[37] F. Lu, H. Zhang, and C. Mi. A Review on the Recent Development of Capacitive Wireless Power Transfer Technology. *Energies*, 10(11), 2017.

[38] F. Lu, H. Zhang, and C. Mi. A Two-Plate Capacitive Wireless Power Transfer System for Electric Vehicle Charging Applications. *IEEE Transactions on Power Electronics*, 33(2):964–969, 2018.

[39] X. Lu, P. Wang, D. Niyato, D. I. Kim, and Z. Han. Wireless networks with rf energy harvesting: A contemporary survey. *IEEE Communications Surveys Tutorials*, 17(2):757–789, Sept 2015.

[40] K. A. U. Menon, A. Gungi, and B. Hariharan. Efficient wireless power transfer using underground relay coils. In *International Conference on Computing, Communications and Networking Technologies (ICCCNT)*, 2014.

[41] C. Park and P. H. Chou. Ambimax: Autonomous energy harvesting platform for multi-supply wireless sensor nodes. In *2006 3rd Annual IEEE Communications Society on Sensor and Ad Hoc Communications and Networks*, pages 168–177, Sept 2006.

[42] V. Raghunathan, A. Kansal, J. Hsu, J. Friedman, and M. Srivastava. Design considerations for solar energy harvesting wireless embedded systems. In *IPSN 2005. Fourth International Symposium on Information Processing in Sensor Networks, 2005.*, pages 457–462, April 2005.

[43] M. Raju. Energy Harvesting. http://www.ti.com/corp/docs/landing/cc430/graphics/slyy018_20081031.pdf, 2008.

[44] A. S. Rekhi, B. T. Khuri-Yakub, and A. Arbabian. Wireless Power Transfer to Millimeter-Sized Nodes Using Airborne Ultrasound. *IEEE Transactions on Ultrasonics, Ferroelectrics, and Frequency Control*, 64(10):1526–1541, 2017.

[45] J. Rigden. *Macmillan Encyclopedia of Physics*. Simon & Schuster Macmillan, 1996.

[46] A. Sample and J. R. Smith. Experimental results with two wireless power transfer systems. In *2009 IEEE Radio and Wireless Symposium*, pages 16–18, Jan 2009.

[47] T. Sasatani, M. J. Chabalko, Y. Kawahara, and A. P. Sample. Multimode quasistatic cavity resonators for wireless power transfer. *IEEE Antennas and Wireless Propagation Letters*, 16:2746–2749, 2017.

[48] L. Shi, Z. Kabelac, D. Katabi, and D. Perreault. Wireless Power Hotspot That Charges All of Your Devices. In *Proc. of ACM MobiCom*, 2015.

[49] H. A. Sodano, G. Park, and D. J. Inman. Estimation of electric charge output for piezoelectric energy harvesting. *Strain*, 40(2):49–58, May 2004.

[50] STMicroelectronics. Calibrating STM32F0x1, STM32F0x2 and STM32F0x8 lines internal RC oscillators, 2015.

[51] J. B. Su. 2 Reasons Why Apple Canceled Its AirPower Wireless Charging Mat: Analysis. https://www.forbes.com/sites/jeanbaptiste/2019/04/06/the-2-reasons-why-apple-canceled-its-airpower-wireless-charging-mat-analysis/, 2019.

[52] H. Tabassum, E. Hossain, A. Ogundipe, and D. I. Kim. Wireless-powered cellular networks: key challenges and solution techniques. *IEEE Communications Magazine*, 53(6):63–71, 2015.

[53] V. Talla, B. Kellogg, S. Gollakota, and J. R. Smith. Battery-free cellphone. *Proc. ACM Interact. Mob. Wearable Ubiquitous Technol.*, 1(2):25:1–25:20, June 2017.

[54] V. Talla, B. Kellogg, B. Ransford, S. Naderiparizi, S. Gollakota, and J. R. Smith. Powering the Next Billion Devices with Wi-fi. In *Proc. of ACM CoNEXT*, 2015.

[55] E. J. Wang, M. Sharma, Y. Zhao, and S. N. Patel. CASPER: Capacitive Serendipitous Power Transfer for Through-body Charging of Multiple Wearable Devices. In *Proc. of ACM ISWC*, 2018.

[56] WIRED. Batteries still suck, but researchers are working on it.

[57] World Power Consortium. Qi Wireless power specification, 2008.

[58] H. Zhang, F. Lu, H. Hofmann, W. Liu, and C. C. Mi. A Four-Plate Compact Capacitive Coupler Design and LCL-Compensated Topology for Capacitive Power Transfer in Electric Vehicle Charging Application. *IEEE Transactions on Power Electronics*, 31(12):8541–8551, 2016.